Energy Balance Climate Modelling with Radiative Forcing and Deep-Ocean Heat Uptake

Wuhua Zhu
BASIS INTERNATIONAL SCHOOL PARK LANE HARBOUR
Guangzhou, China
wuhua_zhu@hotmail.com

January 30, 2026

Abstract

This study uses an energy balance model (EBM) to simulate changes in the global mean surface air temperature. The model incorporates radiative forcing from greenhouse gases, atmospheric aerosols, and volcanic aerosols, and is extended to include heat exchange between the Earth's surface and the deep ocean in order to represent the ocean's role as a heat reservoir.

Simulations were performed using two model configurations: a baseline model without deep ocean heat uptake and an extended model that includes deep ocean dynamics. The simulated surface temperature anomalies were compared with observational data to assess model performance. The inclusion of deep ocean heat uptake improves agreement between simulated and observed temperature anomalies. Using mean absolute error (MAE) as a performance metric, the extended model produces lower error than the baseline configuration.

The model is further used to examine the effects of changes in radiative forcing parameters and climate feedback strength on temperature response. In addition, the physical implications and limitations of several global cooling strategies are discussed within the simplified modeling framework.

Overall, the results highlight the importance of deep ocean heat exchange in regulating surface temperature changes and demonstrate that relatively simple energy balance models can capture key features of the global climate response to external forcing.

1 Introduction

In the summer of 2021, my mother's hometown suffered a once-in-a-century flood, with daily rainfall almost reaching the local annual average. The town was submerged, and the post-disaster scene was shocking. In August 2025, I personally witnessed a super typhoon in Sanya destroying the tranquil island in an instant. These two extreme weather events made me deeply aware of the ferocity of natural forces and the imminent threat of climate change, and also made me determined to use my knowledge to understand and even attempt to predict these phenomena.

Recent extreme weather events have highlighted the direct impacts of strong storms on populated regions and raised public interest in understanding climate drivers. In late September 2025, Super Typhoon Ragasa—a powerful tropical cyclone in the Northwest Pacific—approached southern China and made landfall in Guangdong Province, bringing heavy winds, intense rainfall, and extensive disruptions to transportation and daily life in the Pearl River Delta and surrounding areas Rag [2025]. Winds exceeded 140 kph near landfall and authorities issued the highest tropical cyclone warnings as coastal cities faced flood risks and storm surge warnings. Such events motivate further inquiry into the mechanisms that influence climate variability and extreme weather patterns.

Earth's climate is largely affected by the balance between energy received from the Sun and energy reemitted into space. This balance is captured by an energy balance model, which incorporates the effects of radiative forcing on Earth's surface temperature. Changes in radiative forcing arise from both natural and anthropogenic sources and have been shown to significantly alter climate dynamics Shindell [2013].

Earth reaches radiative equilibrium and a corresponding planetary equilibrium temperature when net radiative forcing is zero. This equilibrium can be disrupted by greenhouse gases, which allow short-wave solar radiation to pass through Earth's atmosphere while inhibiting the escape of long-wave radiation emitted by the Earth's surface Wild [2013]. This trapped radiation produces positive radiative forcing and leads to an increase in global surface temperature. Conversely, most atmospheric aerosols produce negative radiative forcing by reflecting incoming solar radiation back into space, thereby cooling the Earth's surface Charlson [1992].

In addition to radiative forcing, Earth's climate is strongly influenced by the ocean's ability to absorb and store heat. The deep ocean, in particular, absorbs a substantial fraction of excess heat due to its large heat capacity, which exceeds that of the atmosphere, land surface, and upper ocean combined Geoffroy et al. [2013]. This heat uptake acts to moderate the rate of surface temperature increase Menzel and Merlis [2019].

This study models changes in Earth's global mean surface air temperature by incorporating radiative forcing from greenhouse gases, atmospheric aerosols, and heat exchange with the deep ocean.

2 Model Formulation

The model considered in this study is an energy balance model designed to describe Earth's global mean surface temperature. This class of models is based on the fundamental physical principle that changes in Earth's internal energy are equal to the difference between energy received by and energy emitted from the Earth's surface. Mathematically, this relationship can be expressed as

$$\text{Heat content} = \text{Heat capacity} \times \text{Temperature} = C\,T, \tag{1}$$

where C denotes the effective heat capacity of the climate system and T represents the global mean surface temperature.

Assuming that Earth's heat capacity C is constant and differentiating Eq. (1) with respect to time t, a preliminary energy balance equation is obtained as

$$C\frac{dT}{dt} = E_{\text{in}} - E_{\text{out}}, \tag{2}$$

where E_{in} and E_{out} represent the average incoming and outgoing energy fluxes per unit surface area of the Earth, respectively.

The final form of the model is derived by decomposing the energy fluxes into specific physical processes that separately influence the energy received or retained by the Earth and the energy emitted from the system. The incoming energy term is expressed as

$$E_{\text{in}} = E_{\text{sol}} + E_{\text{gas}} + E_{\text{vol}} + E_{\text{aer}}, \tag{3}$$

while the outgoing energy term is given by

$$E_{\text{out}} = G(T) + E_{\text{ocean}}. \tag{4}$$

Here, E_{sol} represents incoming solar radiation, E_{gas} accounts for radiative forcing due to greenhouse gases, E_{vol} and E_{aer} represent radiative effects associated with volcanic and anthropogenic aerosols, respectively. The function $G(T)$ describes outgoing longwave radiation as a function of temperature, and E_{ocean} represents heat exchange between the surface and the deep ocean.

2.1 Solar Radiation (E_{sol})

The incoming solar energy received by the Earth, denoted by E_{sol}, is estimated by approximating the Earth as a sphere and assuming that solar radiation is emitted in parallel rays. Under these assumptions, the effective cross-sectional area intercepting solar radiation is circular, as illustrated in Fig. 1.

Figure 1: Schematic illustration of the simplified solar radiation model.

Under this geometric approximation, the total solar energy intercepted by the Earth is given by $S_0\pi R_e^2$, where S_0 denotes the solar constant and R_e is the radius of the Earth. This energy is distributed over the entire surface area of the Earth, $4\pi R_e^2$. Consequently, the average incoming solar radiation per unit surface area is

$$\frac{S_0\pi R_e^2}{4\pi R_e^2} = \frac{S_0}{4}. \tag{5}$$

A fraction of the incoming radiation is reflected back into space due to the Earth's albedo, denoted by α. Accounting for this effect, the net solar radiation absorbed by the Earth is expressed as

$$E_{\text{sol}} = \frac{(1-\alpha)S_0}{4}, \tag{6}$$

where $\alpha \approx 0.3$ and $S_0 \approx 1368\ \text{W m}^{-2}$.

2.2 Greenhouse Effects (E_{gas})

Greenhouse gases, in particular carbon dioxide (CO_2), methane (CH_4), and nitrous oxide (N_2O), partially inhibit the escape of longwave radiation emitted from the Earth's surface into space. This trapped radiation leads to an increase in surface temperature and is commonly represented in climate models through radiative forcing terms.

In this model, the radiative forcing contributions of the three major greenhouse gases are parameterized using empirical relationships reported in the literature. The corresponding radiative forcing equations and associated constants are summarized in Table 1.

Table 1: Radiative forcing parameterizations for CO_2, CH_4, and N_2O, adapted from **?**.

Gas	Radiative forcing equation	Constants
CO_2	$\Delta F_{CO_2} = \alpha \ln\left(\frac{C}{C_0}\right) + \beta\left(\sqrt{C} - \sqrt{C_0}\right)$	$\alpha = 4.841,\ \beta = 0.0906$
CH_4	$\Delta F_{CH_4} = \alpha\left(\sqrt{M} - \sqrt{M_0}\right) - f(M, N_0) - f(M_0, N_0)$	$\alpha = 0.036$
N_2O	$\Delta F_{N_2O} = \alpha\left(\sqrt{N} - \sqrt{N_0}\right) - f(M_0, N) - f(M_0, N_0)$	$\alpha = 0.12$

Here, C, M, and N denote the atmospheric concentrations of CO_2, CH_4, and N_2O, respectively, while C_0, M_0, and N_0 represent their corresponding pre-industrial reference concentrations. The overlap function $f(M, N)$ accounts for spectral interactions between methane and nitrous oxide and is defined following established formulations in radiative forcing studies.

The total additional energy retained by the Earth due to greenhouse gases is then expressed as the sum of the individual radiative forcing contributions,

$$E_{\text{gas}} = \Delta F_{CO_2} + \Delta F_{CH_4} + \Delta F_{N_2O}. \tag{7}$$

2.3 Volcanic Aerosols (E_{vol})

Aerosols emitted during volcanic eruptions reduce the amount of solar radiation reaching the Earth's surface by reflecting incoming radiation back into space. This process leads to a temporary cooling effect and is incorporated into the model through the following system of equations:

$$\frac{d\,\text{OT}^{\text{vol}}}{dt} = E_{\text{vol}}^{\text{src}} - \frac{1}{\tau^{\text{vol}}}\,\text{OT}^{\text{vol}}, \tag{8}$$

$$E_{\text{vol}} = c^{\text{vol}}\,\text{OT}^{\text{vol}}, \tag{9}$$

where OT^{vol} denotes the optical thickness of volcanic aerosols, $E_{\text{vol}}^{\text{src}}$ represents the aerosol injection rate, τ^{vol} is the characteristic decay timescale, and E_{vol} (W m^{-2}) denotes the radiative forcing contribution associated with volcanic aerosols.

2.4 Anthropogenic Aerosols ($E_{\mathbf{aer}}$)

Anthropogenic aerosols, predominantly sulphur dioxide emissions, exert a radiative forcing effect similar to that of volcanic aerosols by reflecting solar radiation back into space. The contribution of human-caused aerosols to the Earth's energy balance is parameterized as

$$E_{\text{aer}} = c^{\text{aer}}\big(E^{\text{SO}_2}(t) - E^{\text{SO}_2}(0)\big), \tag{10}$$

where $E^{\text{SO}_2}(t)$ ($10^9\,\text{kg}\,\text{yr}^{-1}$) denotes the mass of sulphur dioxide emitted at time t, $E^{\text{SO}_2}(0)$ is the corresponding pre-industrial emission level, and c^{aer} is a dimensionless scaling coefficient.

2.5 Outgoing Longwave Radiation

In typical energy balance models, the Earth is approximated as a grey body that emits longwave radiation according to the Stefan–Boltzmann law,

$$j^* = \sigma\varepsilon T^4, \tag{11}$$

where $\sigma = 5.6703 \times 10^{-8}\,\text{W}\,\text{m}^{-2}\,\text{K}^{-4}$ is the Stefan–Boltzmann constant, ε is the effective emissivity of the Earth ($0 < \varepsilon < 1$), and T denotes the global mean surface temperature.

Empirical observations indicate that the blackbody approximation alone does not fully capture the Earth's outgoing radiation response. Instead, a linear approximation of the outgoing radiative flux is commonly adopted Kaper and Engler [2013]. This approximation is obtained by performing a first-order Taylor expansion of $G(T)$ about the pre-industrial equilibrium temperature $T_0 = 14°\text{C}$:

$$G(T) \approx G(T_0) + G'(T_0)(T - T_0) = -A - BT, \tag{12}$$

where $B < 0$ is the climate feedback parameter ensuring model stability and A ($\text{W}\,\text{m}^{-2}$) is a constant determined by imposing pre-industrial energy balance.

Under pre-industrial equilibrium conditions, the net energy balance satisfies

$$E_{\text{in}} = E_{\text{out}}, \tag{13}$$

which yields

$$A = \frac{S_0(1-\alpha)}{4} + BT_0 \approx 221.2\ \text{W}\,\text{m}^{-2}. \tag{14}$$

A substantial fraction of excess energy in the Earth's climate system is absorbed and stored by the deep ocean, typically at depths greater than 500 m. Owing to its large heat capacity, the deep ocean acts as a long-term heat reservoir and moderates the rate of increase in surface temperature. This heat exchange between the surface and deep ocean is incorporated into the model through the following parameterization:

$$E_{\text{ocean}} = \gamma\big(T_{\text{deep}} - T_{\text{surface}}\big), \tag{15}$$

where T_{surface} denotes the surface ocean temperature (at depths shallower than 500 m), T_{deep} represents the temperature of the deep ocean, and γ ($\text{W}\,\text{m}^{-2}\,\text{K}^{-1}$) is an empirically derived coupling coefficient that governs the rate of heat exchange between the surface and deep ocean layers.

2.6 Final Model

Combining the parameterizations for incoming solar radiation, greenhouse gas forcing, aerosol effects, outgoing longwave radiation, and deep ocean heat uptake, the final energy balance model governing the evolution of the global mean surface air temperature is expressed as

$$C\frac{dT}{dt} = \frac{S_0(1-\alpha)}{4} - (A - BT) - E_{\text{ocean}} + \Delta F_{CO_2} + \Delta F_{CH_4} + \Delta F_{N_2O} + E_{\text{vol}} + E_{\text{aer}}, \tag{16}$$

where C denotes the effective heat capacity of the climate system and T represents the global mean surface air temperature. Descriptions, units, and physical interpretations of all model variables and parameters are provided in Appendix B.

3 Data and Methods

The energy balance model described in Section 2 was implemented as a numerical simulation using Python in a Jupyter notebook environment. The simulation was executed on the Google Colab platform, and the source code is provided in Appendix D. Model inputs consist of time series data for atmospheric greenhouse gas concentrations, volcanic and anthropogenic aerosol emissions, and observed global mean surface air temperature used for model validation.

Atmospheric concentrations of carbon dioxide (CO_2), methane (CH_4), and nitrous oxide (N_2O) were obtained from two primary sources. Recent observational estimates covering the period from 1979 to 2019 were sourced from the National Oceanic and Atmospheric Administration (NOAA). Earlier estimates extending back to year 1 AD were obtained from ice core records collected at Law Dome, Antarctica. These datasets provide annual mean concentrations of CO_2 (ppm) and CH_4 and N_2O (ppb), which were used as inputs for the radiative forcing calculations.

Data for sulphur dioxide (SO_2) emissions and volcanic aerosol loading were obtained from the Carbonator Climate Model. This dataset provides annual values of visible aerosol optical depth at a wavelength of 550 nm, as well as global SO_2 emissions reported on 5- and 10-year intervals. Annual SO_2 emission levels were estimated by linear interpolation between consecutive reported values. The resulting time series is illustrated in Figure 2.

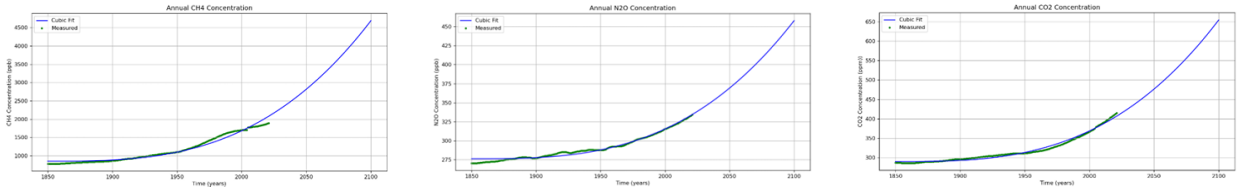

(a) CH_4 concentration (b) N_2O concentration (c) CO_2 concentration

Figure 2: Annual atmospheric concentrations of CO_2, CH_4, and N_2O.

Model validation was performed using observational surface temperature data from NASA's Land–Ocean Temperature Index (LOTI). This dataset reports annual global mean temperature anomalies relative to the pre-industrial baseline period (1850). To obtain absolute surface air temperatures, a constant offset of 14.15 °C was added to the reported anomalies. The resulting temperature series was compared with simulated model outputs to assess model performance.

4 Results

Initial simulations were conducted using an energy balance model that did not incorporate heat exchange between the surface and the deep ocean. An extended version of the model, which includes deep ocean heat uptake, was then evaluated to assess the impact of this process on model performance.

Simulated and observed global mean surface temperature anomalies were compared for the two model configurations. Temperature anomalies are defined relative to the pre-industrial baseline (1850), with an absolute reference temperature of 14.15 °C used to compute annual simulated and observed temperatures.

Model performance was quantified using the mean absolute error (MAE) between simulated and observed temperature anomalies. For the baseline model excluding deep ocean heat uptake, the MAE was found to be 0.167 °C. In contrast, the extended model incorporating deep ocean dynamics achieved a reduced MAE of 0.154 °C.

These results demonstrate that inclusion of deep ocean heat exchange improves agreement between simulated and observed surface temperature anomalies.

5 Model Evaluation

This section presents a qualitative evaluation and physical interpretation of the model behaviour, focusing on how different radiative forcings influence the mean global surface temperature, the timescale over which the system responds to these forcings, and the transfer of energy between the surface and the deep ocean. The implications of these behaviours for different global cooling strategies are also examined.

A series of diagnostic plots is used to analyse the response of the model to changes in radiative forcing from CO_2, CH_4, N_2O, SO_2, and volcanic aerosols, alongside the corresponding surface and deep ocean temperature anomalies, as shown in Figure A1.

Sensitivity analyses are performed by varying forcing coefficients to explore both short- and long-term temperature responses and the conditions under which the model approaches energy balance.

Since aerosols produce negative radiative forcing, their forcing coefficients are negative, and reducing their magnitude leads to a decrease in temperature. It can be observed that decreasing the forcing coefficient associated with volcanic emissions primarily affects temperature in the short term and has a limited impact on long-term temperature trends, as shown in Figure A2(b). In contrast, decreasing the forcing coefficient associated with SO_2 results in a reduction in temperature over the long term, as shown in Figure A2(d). When all forcing coefficients are set to zero, the model reaches energy balance and a constant temperature is obtained, as shown in Figure A2(e) and Figure A2(f).

The time required for surface temperature to respond to changes in radiative forcing also depends strongly on the heat capacity of the surface and deep ocean, as well as the rate at which heat is transferred into the ocean and emitted into space. Another plotting feature in the Jupyter notebook is used to demonstrate this behaviour. It visualises surface and deep ocean temperature anomalies alongside the effective temperature anomaly resulting from incoming solar energy and outgoing blackbody radiation. Interactive sliders allow the heat capacity of the surface and deep ocean to be adjusted, as well as the rate of heat transfer between the ocean and the atmosphere.

The heat capacity of a reservoir determines the amount of heat required to produce a change in temperature. Specifically, the surface heat capacity affects how sensitive the surface temperature is

to changes in radiative forcing. This effect can be highlighted by increasing the albedo to simulate a planet that reflects a large proportion of incoming solar radiation (for instance, an ice-covered planet). This reduces the constant incoming heat energy, such that perturbations due to radiative forcing imbalances can be accentuated. When the surface heat capacity is reduced, greater dips in surface temperature are observed following volcanic eruptions, demonstrating the high sensitivity of surface temperature to changes in radiative forcing, as shown in Figure A3(b). A similar, though slightly delayed, effect is observed in the deep ocean temperature when the deep ocean heat capacity is also reduced, as shown in Figure A3(c).

The climate feedback parameter represents a form of negative feedback and, within the compartmental model, describes the rate at which heat energy is transferred to the sink. As a result, the climate feedback parameter determines how efficiently the Earth can naturally cool by emitting heat energy into space. Increasing the absolute value of this parameter leads to a more stable system in which the overall temperature of both the surface and deep ocean is less affected by positive radiative forcing, thereby slowing global warming. In this case, temperature increases occur more gradually and remain below 2°C until approximately the year 2600, as shown in Figure A4(a). Conversely, decreasing the absolute value of the climate feedback parameter reduces system stability, accelerating the effects of global warming and causing the surface temperature to rise above 2°C by the year 2017, as shown in Figure A4(b).

6 Implications and Limitations

The goal of the Paris Agreement is to ensure that the rise in mean global temperature remains below 1.5°C above pre-industrial levels United Nations [2015]. Model projections indicate that if anthropogenic greenhouse gas emissions continue to increase following the observed cubic trends shown in Figure A5(a), (b), and (c), the global mean surface temperature will exceed the 1.5°C threshold by approximately the year 2040, as shown in Figure A1(b).

CO_2 is well known to have the strongest impact on climate among anthropogenic greenhouse gases. Figure A1(b) shows that CO_2 produces the greatest positive radiative forcing and thus exerts a larger influence on rising temperature than CH_4 and N_2O. However, the model fails to accurately simulate the effects of reducing future CO_2 emissions, as it does not explicitly consider the carbon cycle. Incorporating the carbon cycle would allow the absorption and release of carbon and CO_2 by the upper and deep ocean, as well as uptake by vegetation and soils, followed by the delayed release of CO_2 back into the atmosphere. This would make it possible to simulate delayed radiative forcing associated with dormant CO_2 and carbon stored within the Earth system.

As a result, the model produces an unrealistic projection in which surface temperatures would cease to rise if net-zero greenhouse gas emissions were achieved in 2021, maintaining a stable equilibrium temperature approximately 1°C above the pre-industrial level. More advanced climate models demonstrate that temperatures would continue to increase for some time after net-zero emissions are reached, before stabilising at a new equilibrium. This equilibrium would depend primarily on atmospheric CO_2 concentrations and the amount of carbon stored in the ocean and terrestrial reservoirs at the time net-zero emissions are achieved. This suggests that realistic global cooling strategies would require the removal of CO_2 from the atmosphere to prevent temperatures from rising beyond 1.5°C.

The IPCC targets the removal of 100–1000 Gt of CO_2 within this century in order to limit warming to a 1.5°C equilibrium temperature National Research Council [2015]. Selecting 500 Gt as a representative target, a rough estimate indicates that this would correspond to an atmospheric CO_2 concentration of approximately 316.8 ppm by the year 2100. Further details of this calculation

are provided in Appendix C.

By projecting atmospheric CO_2 concentrations to decrease linearly from 414 ppm in 2021 to 316.8 ppm in 2100, the model simulates a temperature increase that remains well below that envisioned by the IPCC, as shown in Figure 3. However, the model cannot accurately assess global cooling strategies that involve direct extraction of CO_2 from the atmosphere, such as bioenergy with carbon capture and storage (BECCS) and direct air capture, as it does not represent the persistence of CO_2 and carbon within the climate system. As a result, the model would significantly underestimate future temperature increases following reductions in atmospheric CO_2 levels.

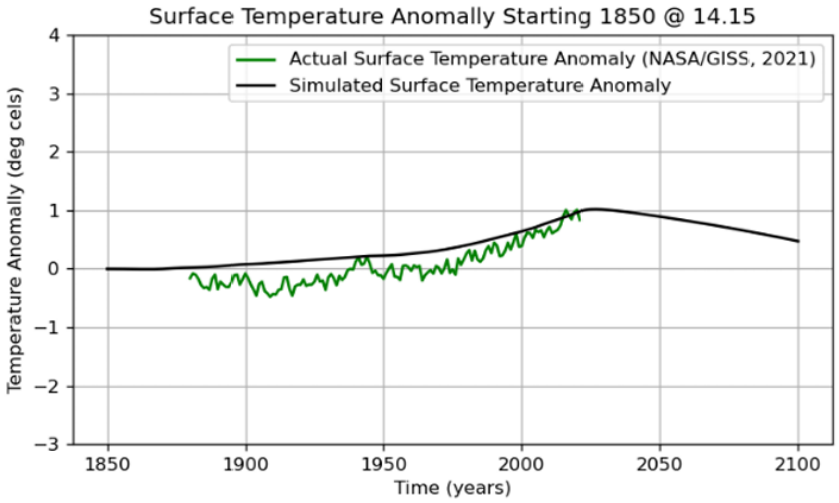

(a) Simulated temperature decrease as a result of removing 500 Gt of CO2 from the atmosphere at a linear rate from 2021-2100.

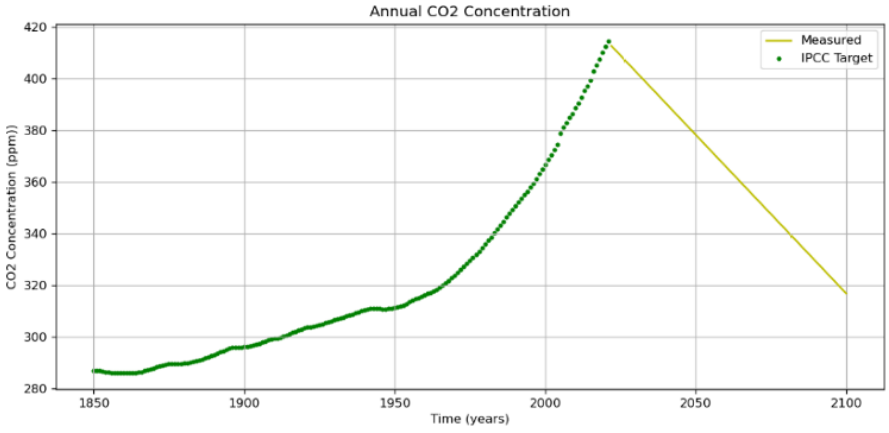

(b) Linear projection of CO2 concentration corresponding to the IPCC target of removing 500Gt of CO2 from the atmosphere by 2100 starting from the year 2021.

Figure 3

Solar geoengineering refers to a class of climate engineering approaches aimed at reducing the amount of solar energy entering the Earth's climate system. One such method, known as Marine Cloud Brightening (MCB), involves increasing cloud reflectivity over the oceans, thereby increasing the planetary albedo. Increasing the albedo linearly from 0.31 to 0.35 between 2021 and 2100 simulates MCB counteracting the radiative forcing associated with cubic growth in CO_2 emissions, as shown in Figure 4. However, this approach cannot be extended indefinitely, as albedo is a bounded ratio with an upper limit of 1. MCB may therefore serve as a rapidly effective and relatively inexpensive short-term cooling strategy Hill and Ming [2010], while longer-term solutions

must focus on reversing the greenhouse effect and removing greenhouse gases from the atmosphere.

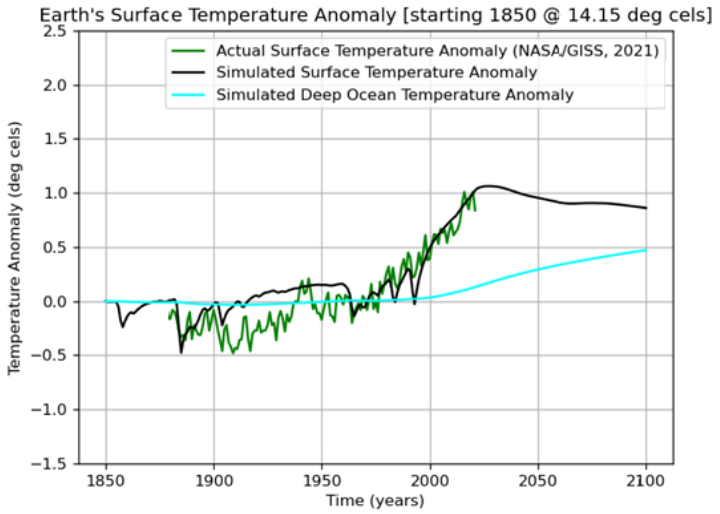

Figure 4

Stratospheric Aerosol Injection (SAI) represents another solar geoengineering approach, in which aerosols (such as sulphur dioxide) are released into the stratosphere to induce negative radiative forcing. Considering only the radiative forcing associated with CO_2 and SO_2, Figure 5 illustrates the SO_2 emission rates required to offset the positive radiative forcing produced by cubic growth in CO_2 emissions. However, studies suggest that SAI may lead to a range of harmful side effects, including changes in rainfall distribution and impacts on water resources in certain regions. MCB may exhibit similar environmental risks associated with increased sulphur emissions, although it is generally considered a safer and more viable alternative.

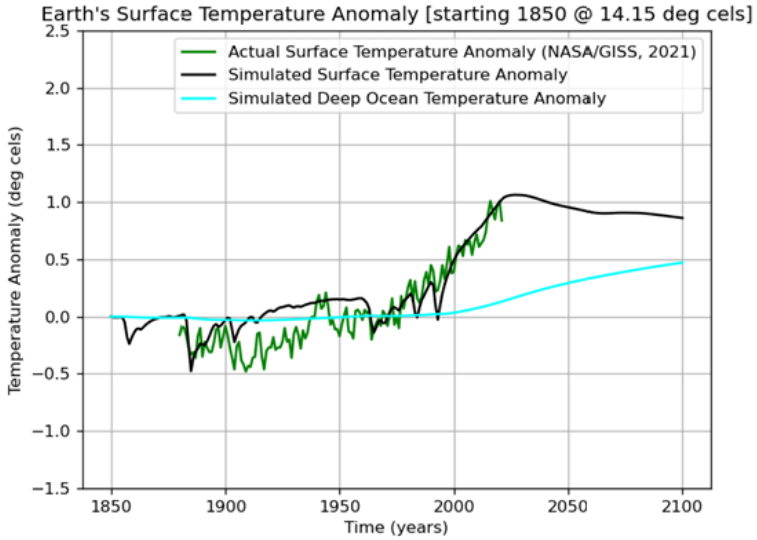

Figure 5

Other global cooling strategies involve enhancing ocean heat uptake. Increasing ocean alkalinity by dispersing pulverised carbonate minerals onto the sea surface is one approach that can increase

the ocean's capacity to absorb heat. Another proposed strategy involves restoring coastal blue carbon ecosystems, such as mangroves and seagrasses, which have the potential to remove substantial amounts of carbon from the atmosphere. These cooling strategies can be partially simulated within the model by increasing the rate of heat transfer between the surface and deep ocean. However, enhanced ocean heat uptake leads to increased ocean temperatures and, consequently, sea level rise. Increasing the ocean feedback parameter from 0.73 to 1.5 and the deep ocean heat capacity from 109 to 120 results in a reduction of the projected surface temperature in 2050 from 1.7°C to 1.4°C, as shown in Figure 6. These results indicate that enhancing ocean heat uptake may reduce surface temperatures, but must be applied with caution due to its potential to accelerate sea level rise.

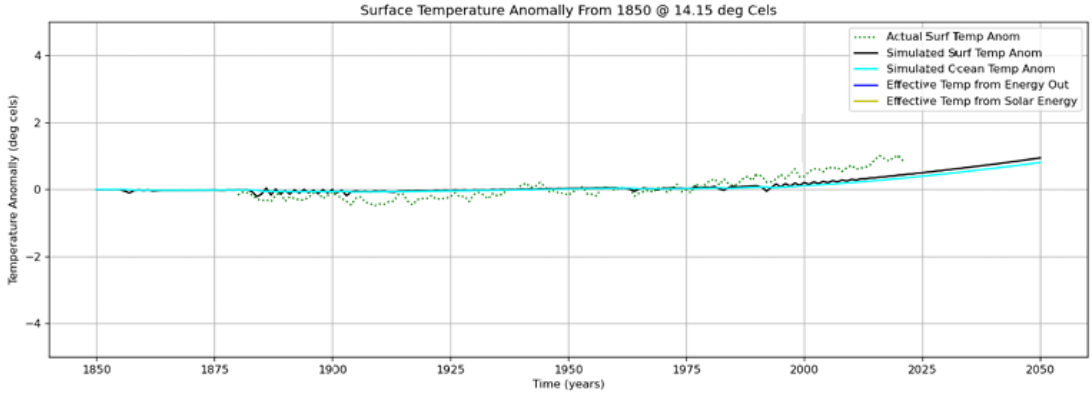

Note. The rate of ocean energy transfer was adjusted from 0.73 to 15 and ocean heat capacity was increased from 109 to 120

Figure 6

7 Conclusion

This study presents a simplified energy balance model for simulating changes in global mean surface air temperature. The model accounts for radiative forcing from greenhouse gases, atmospheric aerosols, and volcanic activity, and includes an extension that represents heat exchange between the surface and the deep ocean.

Comparisons between model configurations show that incorporating deep ocean heat uptake leads to improved agreement with observed surface temperature anomalies. Quantitative evaluation using mean absolute error indicates that the extended model performs better than the baseline model without deep ocean dynamics. This result delivers the role of the ocean in moderating surface temperature changes over time.

The model is also used to explore how variations in radiative forcing and climate feedback parameters influence temperature response. While the simplified framework limits the ability to capture regional effects and complex feedbacks, it provides a clear and interpretable representation of the dominant physical processes governing global temperature change.

Overall, this study demonstrates that relatively simple energy balance models can offer useful insight into the relationship between external forcing, ocean heat uptake, and global temperature evolution. Such models provide a valuable foundation for understanding more complex climate models and for interpreting the physical implications of climate mitigation strategies.

References

Super typhoon ragasa makes landfall in southern china. https://www.reuters.com/business/environment/hong-kong-reopens-after-worlds-most-powerful-cyclone-ragasa-2025-09-25/, 2025. Accessed 25 September 2025.

R. J. Charlson. Climate forcing by anthropogenic aerosols. *Science*, 255:423–430, 1992.

O. Geoffroy, D. Saint-Martin, D. J. L. Olivié, A. Voldoire, G. Bellon, and S. Tyteca. Transient climate response in a two-layer energy-balance model. *Journal of Climate*, 26:1841–1857, 2013.

S. A. Hill and Y. Ming. December climate response to a geo-engineered brightening of subtropical boundary clouds. *AGU Fall Meeting Abstracts*, 2010.

H. Kaper and H. Engler, editors. *Mathematics and Climate*. Society for Industrial and Applied Mathematics, 2013.

M. E. Menzel and T. M. Merlis. Connecting direct effects of co_2 radiative forcing to ocean heat uptake. *Journal of Advances in Modeling Earth Systems*, 11:2163–2176, 2019.

National Research Council. *Climate Intervention: Carbon Dioxide Removal and Reliable Sequestration*. National Academies Press, 2015.

D. Shindell. Radiative forcing in climate change. *Climate Dynamics*, 2013.

United Nations. Paris agreement, 2015.

M. Wild. The global energy balance. *Climate Dynamics*, 2013.

A Additional Figures

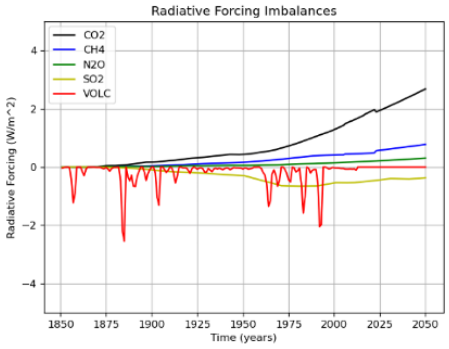

(a) Radiative forcing in Watts per square metre due to aerosols averaged over the entire globe.

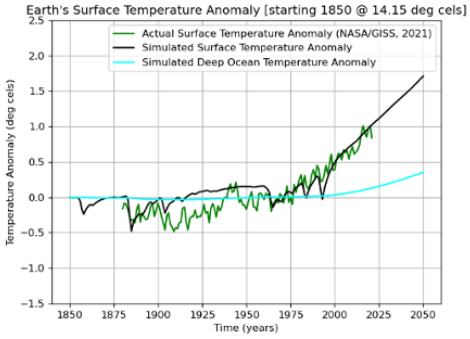

(b) Earth's surface temperature anomaly.

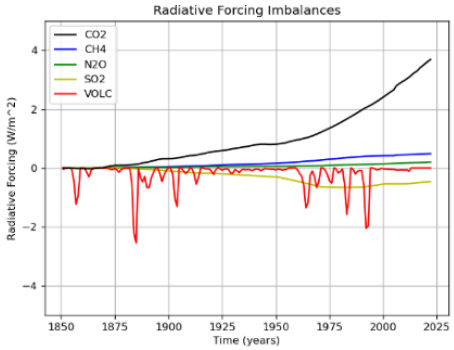

(c) Changes in CO_2 radiative forcing in Watts per square meter.

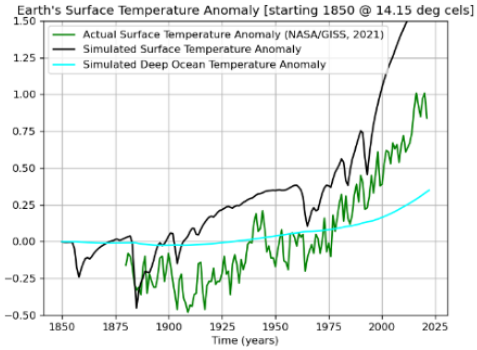

(d) Earth's surface temperature anomaly with changes to CO_2 radiative forcing.

Figure A1: Radiative forcing imbalances and corresponding surface temperature anomalies.

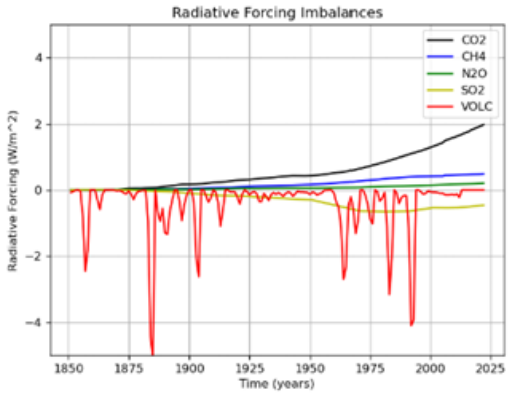

(a) Changes to volcanic aerosol radiative forcing in Watts per square meter.

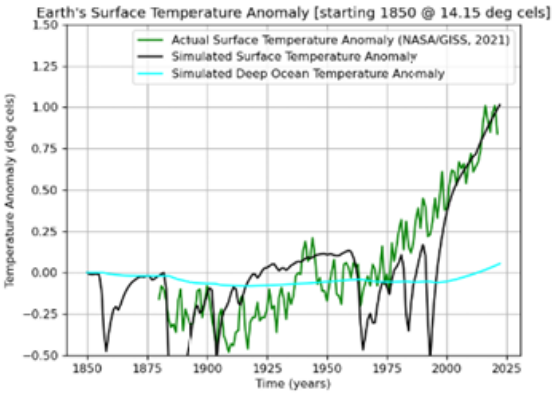

(b) Earth's surface temperature anomaly with changes to volcanic aerosol radiative forcing.

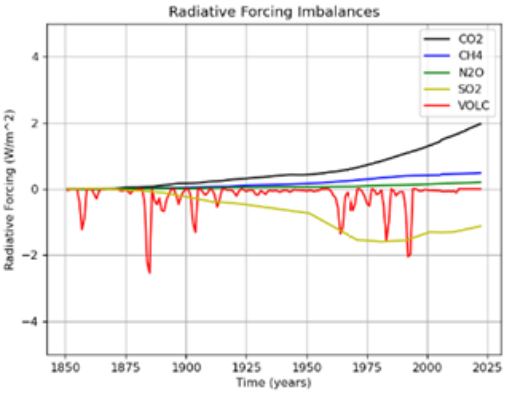

(c) Changes to SO_2 radiative forcing in Watts per square meter.

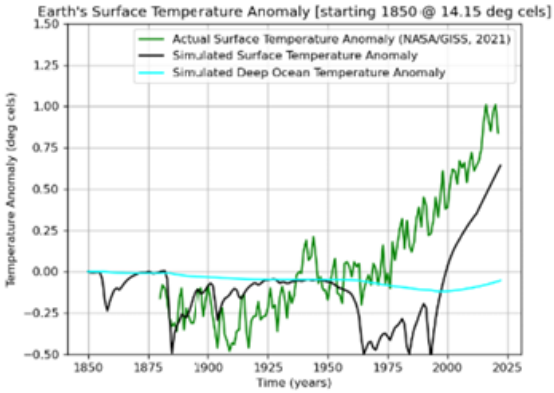

(d) Earth's surface temperature anomaly with changes to SO_2 radiative forcing.

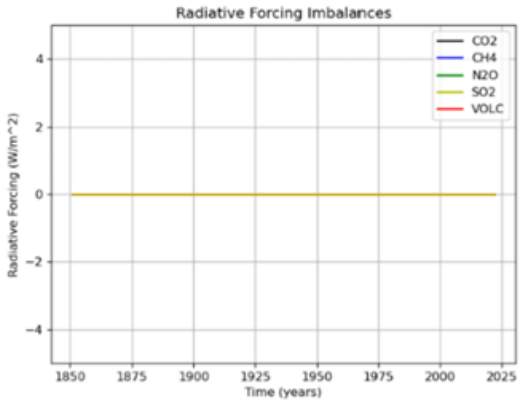

(e) All radiative forcing was set to 0 Watts per square meter.

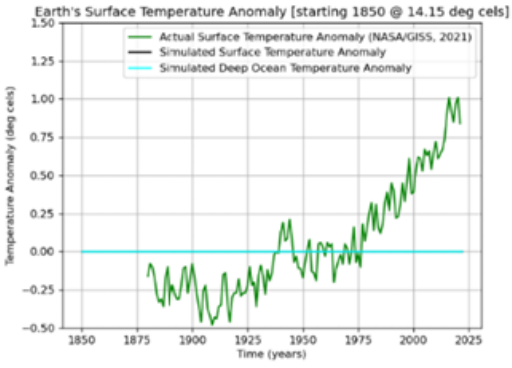

(f) Earth's surface temperature anomaly with all radiative forcing set to 0.

Figure A2: Simulated radiative forcing imbalances and corresponding surface temperature responses. Panels (a), (c), and (e) show changes in radiative forcing due to volcanic aerosols, SO_2, and all forcings set to zero, respectively. Panels (b), (d), and (f) show the resulting surface temperature anomalies under the corresponding forcing configurations.

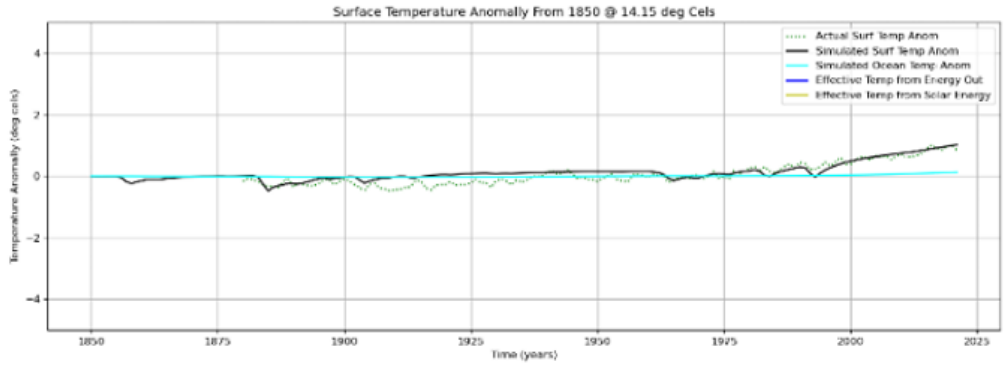

(a) Surface and deep ocean temperature anomaly and effective temperature simulated using empirically determined parameters.

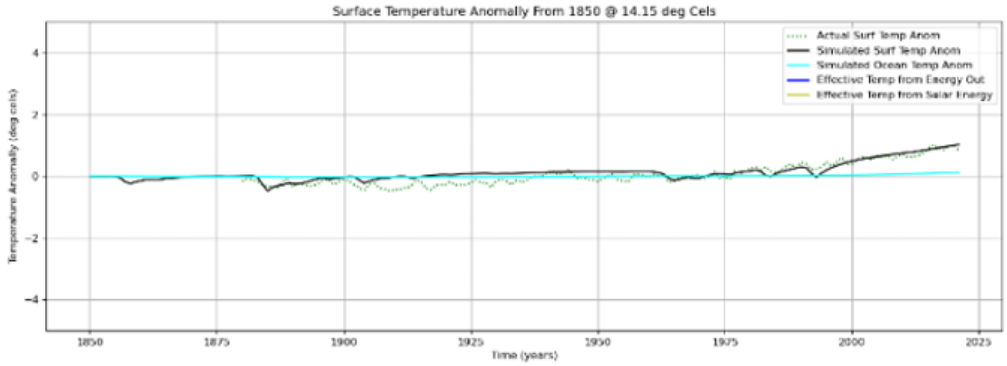

(a) Surface and deep ocean temperature anomaly and effective temperature simulated using empirically determined parameters.

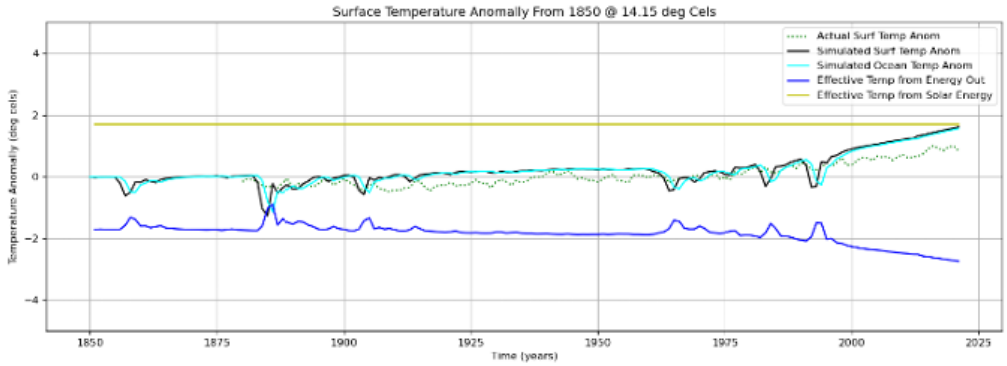

(c) Surface and deep ocean temperature anomaly and effective temperature simulated from setting albedo to 0.99, surface heat capacity to 2 and ocean heat capacity to 1.

Figure A3: Surface and deep ocean temperature anomalies under different model parameter configurations. Panels (a)–(c) show simulations using empirically determined parameters, modified surface heat capacity, and increased albedo, respectively.

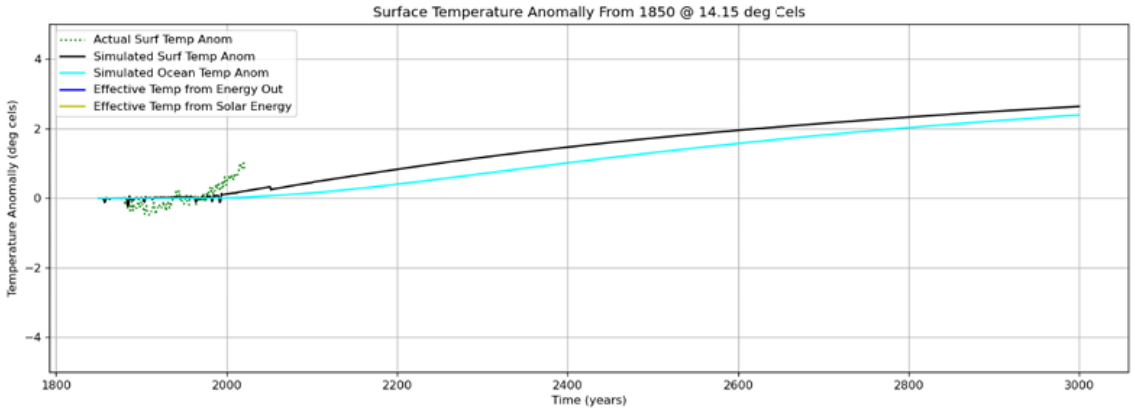

(a) Simulated surface temperature of Earth with the climate feedback parameter lowered from -1.3 to -10.

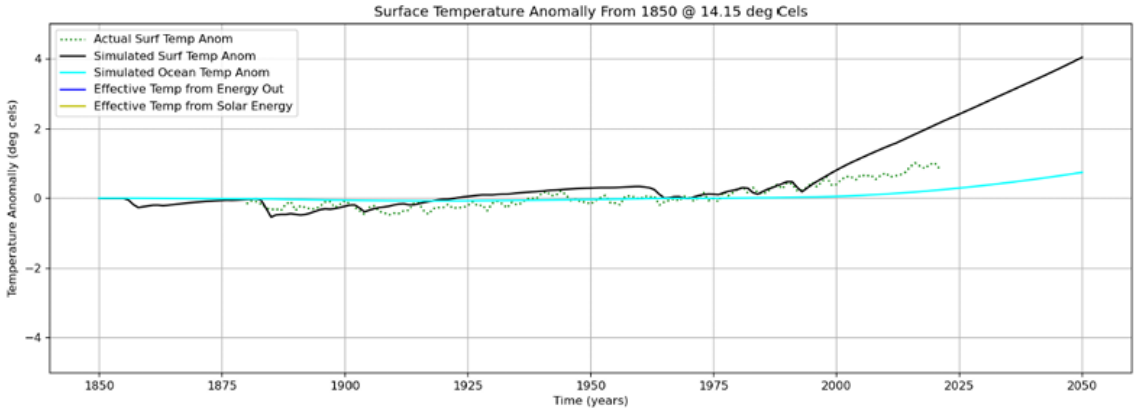

(b) Simulated surface temperature of Earth with the climate feedback parameter lowered from -1.3 to -0.1.

Figure A4: Simulated surface temperature anomalies under different values of the climate feedback parameter. Panel (a) shows the response when the feedback parameter is reduced from -1.3 to -10, while panel (b) shows the response when it is reduced from -1.3 to -0.1.

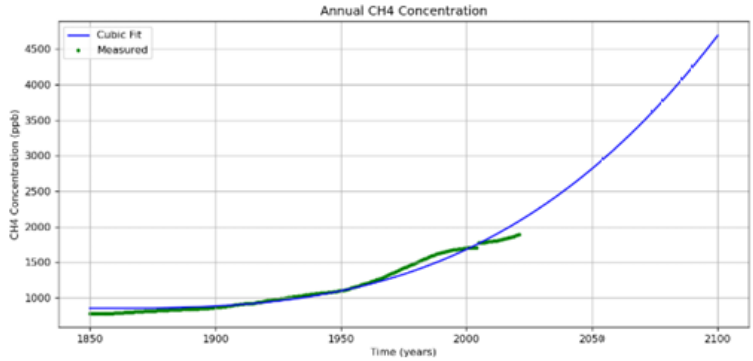

(a) Annual global average concentration of CH4 (ppm) in the atmosphere from 1850-2021 with fitted cubic projections up to the year 2100.

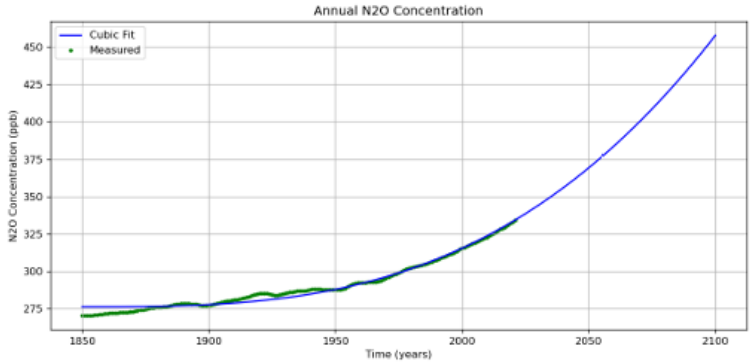

(b) Annual global average concentration of N2O (ppb) in the atmosphere from 1850-2021 with fitted cubic projections up to the year 2100.

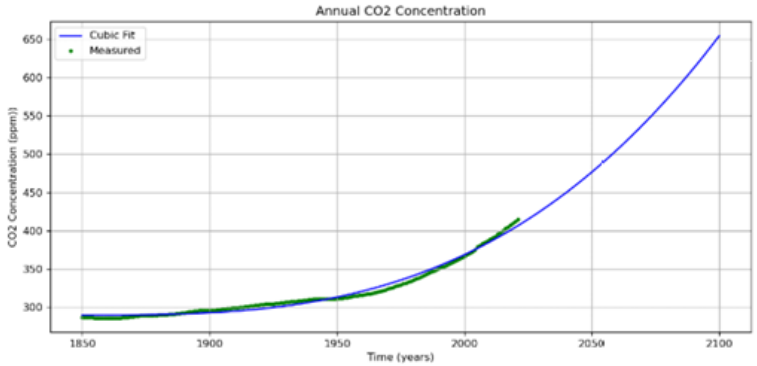

(c) Annual global average concentration of CO2 (ppb) in the atmosphere from 1850-2021 with fitted cubic projections up to the year 2100.

Figure A5

B Additional Table

Table B1: Description, units and dimensions of model variables

Variable	Description	Unit	Dimension
T	Global annual surface temperature	°C	θ
E_{sol}	Solar energy received by Earth	W m^{-2}	M T^{-3}
ΔF_{CO_2}	Radiative forcing of carbon dioxide	W m^{-2}	M T^{-3}
C_{CO_2}	Mass of CO_2	10^9 kg	M
$F_{CO_2}(t)$	Mass of CO_2 emitted per unit time	10^9 kg t^{-1}	M T^{-1}
τ_{CO_2}	Half-life of CO_2 in atmosphere	t^{-1}	T^{-1}
ΔF_{CH_4}	Radiative forcing of methane	W m^{-2}	M T^{-3}
C_{CH_4}	Mass of CH_4	10^9 kg	M
$F_{CH_4}(t)$	Mass of CH_4 emitted per unit time	10^9 kg t^{-1}	M T^{-1}
τ_{CH_4}	Half-life of CH_4 in atmosphere	t^{-1}	T^{-1}
ΔF_{N_2O}	Radiative forcing of nitrous oxide	W m^{-2}	M T^{-3}
C_{N_2O}	Mass of N_2O	10^9 kg	M
$F_{N_2O}(t)$	Mass of N_2O emitted per unit time	10^9 kg t^{-1}	M T^{-1}
τ_{N_2O}	Half-life of N_2O in atmosphere	t^{-1}	T^{-1}
OT^{vol}	Optical thickness due to volcanic aerosols	m	L
E_{vol}	Energy change related to volcanic aerosols	W m^{-2}	M T^{-3}
$E_{SO_2}(t)$	Mass of human aerosol emitted per unit time	10^9 kg t^{-1}	M T^{-1}
$T_{deep-ocean}$	Temperature of deep ocean	°C	θ
$T_{surface-ocean}$	Temperature of surface ocean	°C	θ

Table B2: Description, units and dimensions of model parameters

Parameter	Description	Unit	Dimension
C	Heat capacity of the Earth	W m^{-2} °C	M T$^{-3}\theta^{-1}$
α	Planetary albedo	–	–
S_0	Solar constant	W m^{-2}	M T^{-3}
k_{CO_2}	CO_2 emission constant	10^9 kg t^{-3}	M T^{-3}
k_{CH_4}	CH_4 emission constant	10^9 kg t^{-3}	M T^{-3}
k_{N_2O}	N_2O emission constant	10^9 kg t^{-3}	M T^{-3}
c^{vol}	Volcanic aerosol emission constant	W m^{-3}	M T^{-3} L^{-1}
c^{SO_2}	Human aerosol emission constant	W m^{-2} 10^{-9} kg^{-1} t^{-1}	T^{-2}
A	Linearised outgoing radiation constant	W m^{-2}	M T^{-3}
B	Climate feedback parameter	W m^{-2} °C	M T$^{-3}\theta^{-1}$
γ	Ocean heat uptake coefficient	W m^{-2} °C	M T$^{-3}\theta^{-1}$

C Calculation

The following calculation was used to estimate the mass of carbon dioxide (CO_2) in the atmosphere in 2021, given that the recorded atmospheric concentration was 414 ppm.

The concentration of a solute in parts per million is defined as

$$\text{concentration}_{\text{ppm}} = \frac{\text{mass of solute}_{\text{Gt}}}{\text{mass of solution}_{\text{Gt}}} \times 10^6.$$

Since CO_2 constitutes less than 1% of the total atmospheric mass, the mass of the atmosphere (the solution) was assumed to be constant at 5.148×10^6 Gt. The mass of atmospheric CO_2 in 2021 is therefore approximated as

$$\text{mass of solute} \approx 414 \times 5.148 = 2131.72 \text{ Gt}.$$

Reducing this value by the target removal amount of 500 Gt yields an estimated remaining atmospheric CO_2 mass of

$$\frac{2131.72 - 500}{5.148} = 316.8 \text{ ppm}.$$

This concentration corresponds to the target level required for the global mean surface temperature increase to peak at approximately 1.5°C by the year 2100.

D Code Source

The complete source code used for all models, figures, and simulations is available as a Google Colab notebook at the following link: HERE.